Article

Optical Pushing: A Tool for Parallelized Biomolecule Manipulation

Gerrit Sitters,[1] Niels Laurens,[1] Emilie J. de Rijk,[1] Holger Kress,[2,3] Erwin J. G. Peterman,[1] and Gijs J. L. Wuite[1,*]
[1]Department of Physics and Astronomy and LaserLaB, VU University Amsterdam, Amsterdam, The Netherlands; [2]Experimental Physics I, University of Bayreuth, Bayreuth, Germany; and [3]Department of Applied Physics, Eindhoven University of Technology, Eindhoven, The Netherlands

ABSTRACT The ability to measure and manipulate single molecules has greatly advanced the field of biophysics. Yet, the addition of more single-molecule tools that enable one to measure in a parallel fashion is important to diversify the questions that can be addressed. Here we present optical pushing (OP), a single-molecule technique that is used to exert forces on many individual biomolecules tethered to microspheres using a single collimated laser beam. Forces ranging from a few femtoNewtons to several picoNewtons can be applied with a submillisecond response time. To determine forces exerted on the tethered particles by the laser, we analyzed their measured Brownian motion using, to our knowledge, a newly derived analytical model and numerical simulations. In the model, Brownian rotation of the microspheres is taken into account, which proved to be a critical component to correctly determine the applied forces. We used our OP technique to map the energy landscape of the protein-induced looping dynamics of DNA. OP can be used to apply loading rates in the range of 10^{-4}–10^{6} pN/s to many molecules at the same time, which makes it a tool suitable for dynamic force spectroscopy.

INTRODUCTION

Single-molecule techniques such as tethered-particle motion (TPM) (1), magnetic tweezers (MTs) (2), optical tweezers (OTs) (3), biomembrane-force probe (4), centrifuge force microscopy (CFM) (5), and atomic force microscopy (6) have greatly advanced our ability to quantify the mechanical properties, dynamics, and interactions of biological macromolecules (7–9). Dynamic force spectroscopy, an approach in which molecular interactions are subjected to various loading rates to quantify their energy landscapes, is a particularly popular approach in biophysics (4). Many single-molecule methods that probe one molecule at a time are limited by low experimental throughput, which makes obtaining statistical information over many molecules and identifying rare events challenging. Techniques such as TPM, MTs, and CFM tackle this problem by measuring multiple single molecules in parallel. All these techniques, however, have their limitations: in TPM, no forces are applied, and in CFM and MTs, constant forces are applied that can only be varied on a timescale of seconds. Here we present a bionanosensing method that combines high throughput with rapid force application: optical pushing (OP). OP uses the momentum of laser-generated photons to apply tensions from a few femtoNewtons of up to several picoNewtons to multiple DNA molecules tethered between a surface and microspheres.

Submitted June 24, 2015, and accepted for publication November 17, 2015.

*Correspondence: g.j.l.wuite@vu.nl

Gerritt Sitters and Niels Laurens contributed equally to this article.

Editor: Jennifer Curtis.

0006-3495/16/01/0044/7

MATERIALS AND METHODS

For the implementation of OP, we used a single, collimated laser beam, coupled to an inverted microscope to apply controlled forces to multiple microsphere-tethered biomolecules distributed over a field of view with a size of hundreds of micrometers squared. The setup (Fig. 1) contained three sets of components: the optical pathway of the laser, the flow cell with sample, and the imaging pathway.

As a source of radiation pressure, a collimated laser (YLP-20-LP-IPG; IPG Photonics, Oxford, MA) beam was used with a wavelength of 1070 nm, maximum power of 20 W (power regulation was achieved by a combination of a half-wave plate and a polarizing beam splitter), and a beam diameter of ~70 μm (full width at half-maximum) generated using a telescope consisting of an achromatic lens (focal length = 150 mm) and an aspherical lens (focal length = 4 mm).

The flow cell with sample chamber consisted of a quartz microscope slide and a quartz coverslip separated by parafilm spacers. Quartz was used to minimize sample heating by the laser. Functionalized molecules were attached to both the surface and the microspheres (Fig. 1 *b*) (9).

For imaging, a 455-nm-light-emitting diode (M455L3; IMM Photonics, Unterschleissheim, Germany) was used, coupled into the aspherical lens using a dichroic mirror. The light transmitted by the sample was collected with a long-working-distance air microscope objective (50× NA0.42, No. 58-237; Edmund Optics, York, UK) and imaged, using the tube lens of the microscope, on a complementary metal-oxide semiconductor (CMOS) camera (DCC1545M; Thorlabs, Newton, NJ) (Fig. 1 *c*), which allowed taking images with a frame rate of 25 Hz (full frame). An infrared neutral density filer was placed in front of the camera, to remove remaining laser light. The particles in the images were tracked in three dimensions using a cross-correlation algorithm (x, y), and by comparing the measured radial profile against a database of calibrated radial profiles, made at known heights (z) using a piezo stage (P-517.3CL; Physik Instrumente, Auburn, MA). This resulted in a three-dimensional subpixel precision for the particle tracking of $<$2 nm in x, y and $<$5 nm in the z (see Fig. S1 in the Supporting Material). For stable use of OP it was essential to avoid heating of the objective by the laser, which induced drifting aberrations in the acquired images. The heating was minimized by redirecting the laser light after

http://dx.doi.org/10.1016/j.bpj.2015.11.028

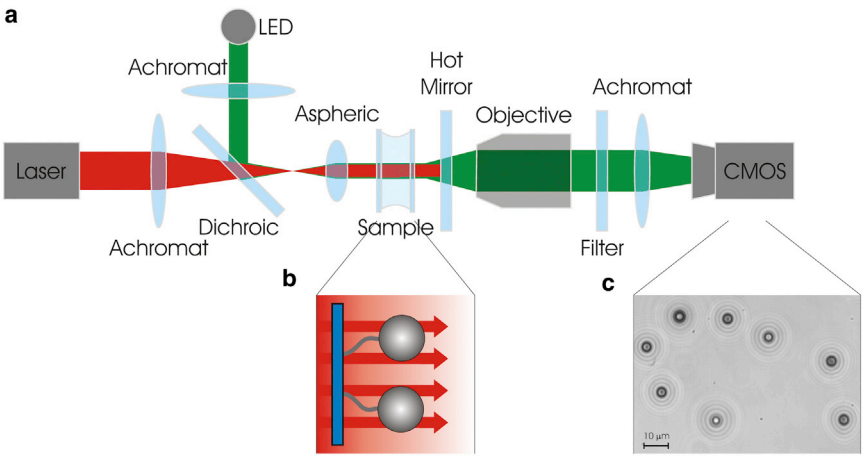

FIGURE 1 (*a*) Schematic drawing of the setup: a 1070 nm laser that is directed through two lenses is used to apply an optical pushing force to microspheres in the sample. Behind the sample, the beam is reflected back using a hot mirror, to prevent heating of the imaging objective. For imaging of the microspheres, the sample is illuminated with a LED. The LED light is transmitted through the hot mirror and imaged on a CMOS camera. (*b*) Biomolecules are tethered to the surface and attached to microspheres. (*c*) Example image of the CMOS camera (25 Hz, 40 ms integration time). The radial ring patterns around the microsphere images are used to determine their distance relative to the surface.

interacting with the sample, before entering the imaging objective, using a hot mirror back into the sample. Because of the divergence of the Gaussian laser beam, the radiation pressure due to the reflected laser light was >1 order-of-magnitude weaker than that due to the direct light.

RESULTS

Validation of the technique

To demonstrate that OP is suitable for the manipulation of tethered molecules, we investigated the restriction of three-dimensional Brownian motion of a single, DNA-tethered (1.1 kbps) microsphere (Ø 2.10 μm polystyrene), with root-mean-square (RMS) displacement detection (Fig. 2). When a laser power of 1.6 W was applied to the sample, the random motion of the microsphere in all three dimensions was restricted. In addition, the distance of the microsphere with respect to the surface (z) increased. Both observations indicate that the radiation pressure of the laser beam actively pushed the microsphere away from the surface. Note that the microsphere found its new equilibrium position, within one camera frame, demonstrating that OP allows switching on and off forces faster than 40 ms (acquisition time of a single camera frame).

The performance of OP on the forces exerted on the biomolecules was determined by measuring and analyzing the Brownian motion of the microspheres. Apart from translational Brownian motion, the microspheres also underwent rotational Brownian motion, which caused them to swivel around their attachment points (see Fig. S2). Because of this swiveling motion, force-calibration methods for tethered microspheres, as used for, e.g., MTs, are not directly

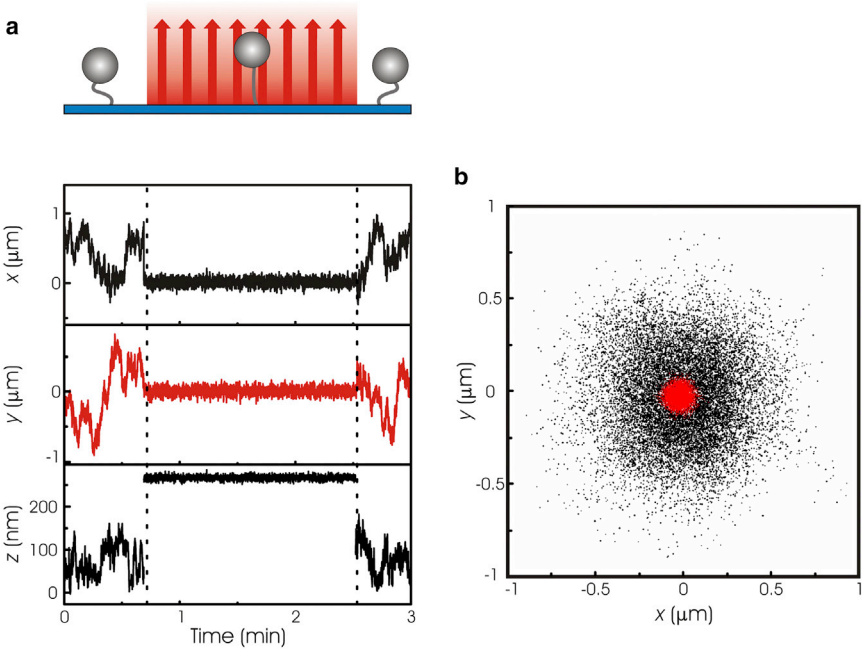

FIGURE 2 Proof of principle of optical pushing. (*a*) Raw motion trace of a DNA (1.1 kbp) tethered microsphere (ϕ 4.26 μm) when there is no laser pushing force and when the laser is set to 2 W (between *dashed lines*). The motion of the microsphere is quenched in all three dimensions when the laser is on. Distances are relative to the DNA-surface anchor point. (*b*) An x,y-scatter plot of the beads position when the laser is off (*black data*) and set to 2 W (*red data*).

applicable to our system (10). In MTs, the paramagnetic microspheres have a fixed alignment with respect to the external magnetic field, which allows neglecting Brownian rotation (11). In the absence of this fixed alignment, the swiveling of the microsphere increases its motion, leading to an underestimation of the force with up to 10% if the swiveling is not taken into account (with DNA tethers that are short compared to the microsphere radius; see Fig. S3). Solving the linearized system of Langevin equations for translation and rotation (Eqs. 1 and 2) (12,13), under the assumption that the exerted force is substantially larger than the thermal fluctuations, yielded an analytical expression for the double-sided power spectrum of the microsphere's motion in the x- and y directions (Eq. 3) (see the Supporting Material for derivation):

$$m\frac{d\vec{v}}{dt} = \vec{F}_{\text{brown}}(t) - \vec{\gamma}\vec{v}(t) + \vec{F}_{\text{ext}}(t), \tag{1}$$

$$I\frac{d\vec{\omega}}{dt} = \vec{T}_{\text{brown}}(t) - \vec{\beta}\vec{\omega}(t) + \vec{T}_{\text{ext}}(t), \tag{2}$$

$$P(f) = 2k_{\text{B}}T\frac{\left(\beta + \gamma\langle z\rangle^2\right)R^2F_{\text{laser}}^2 + \left(\langle z\rangle - R\right)^2\beta^2\gamma(2\pi f)^2}{\left((R-\langle z\rangle)\beta\gamma(2\pi f)^2 + RF_{\text{laser}}^2\right)^2 + \left(2\pi f(R\gamma\langle z\rangle - \beta)F_{\text{laser}}\right)^2}. \tag{3}$$

In Eqs. 1–3, m is the mass of the microsphere, $\vec{v}$ is its velocity, $\vec{F}_{\text{brown}}$ is the random Brownian force, $\vec{\gamma}$ is the effective translational drag coefficient, $\vec{F}_{\text{ext}}$ is the external forces acting on the microsphere, I is the microsphere's moment of inertia, $\vec{\omega}$ is its angular velocity, $\vec{T}_{\text{brown}}$ is the random Brownian torque, $\vec{\beta}$ is the effective rotational drag coefficient, $\vec{T}_{\text{ext}}$ is the external torques acting on the particle, k_B is the Boltzmann's constant, T is the temperature, $\langle z\rangle$ is the average microsphere height, R is the microsphere radius, F_{laser} is the exerted laser force, and f is the frequency. Recently, Daldrop et al. (14) derived a similar analytical expression (Eq. 15 in their article) for the single-sided power spectrum of a sphere undergoing rotation about its tether point. Their expression corresponds closely to our analytical expression (Eq. 3, and see Fig. S3). To confirm the validity of our analytical solution, we compared it to simulations. Simulated data was obtained by implementing an initial microsphere position and rotation, and recursively solving Eqs. 1 and 2 (for full derivation, see the Supporting Material) using randomly varying instantaneous Brownian forces and torques. The difference between the simulated data and the analytically obtained restoring force and torque data (*red*) lies within a few percent (see Fig. S2 *c*). Moreover, the analytical solution of the power spectrum (Eq. 3) agrees with the power spectra of simulated data traces (see Fig. S2 *d*), for forces $F_{\text{laser}} >> F_{\text{brown}}$, confirming that our rotational model is a suitable calibration method for the optical force acting on the biomolecules.

With a calibration method in place, we validated OP and determined what forces could be obtained. Power spectra of DNA tethers attached to microspheres of two different sizes were obtained as a function of laser power and fitted using Eq. 3 (Fig. 3). For both microsphere sizes a linear dependency of force on total laser power was obtained, as expected from the linear dependence of radiation pressure on light intensity (Fig. 3 *b*, *open symbols* and *solid lines*). Moreover, the measured forces match theoretical predictions based on Mie scattering theory (16) (Fig. 3 *b*, *dashed curves*). These measurements demonstrate that our OP instrument is capable of applying forces up to 2.6 pN/W to 4.26-μm microspheres. Due to the Gaussian profile of the laser intensity, the force acting on the tethered microspheres is not constant over the field of view, but follows the illumination profile (see Fig. S4). To account for this, we calibrate the force on each microsphere individually. It is important to note that the maximum measured pushing force ~15 pN is limited by the strength of the dig-antiDIG interaction used to attach the DNA to the surface, not by a physical constraint of our approach. These forces are not as high as forces obtained using OTs on similar microspheres (typically of ~100 pN/Watt (8)). In OP, the maximum force can be readily increased by using different microsphere sizes or composition. Mie scattering theory predicts that the force is approximately fourfold higher when gold-coated (instead of bare) polystyrene microspheres are used (see Fig. S5). Our setup also allows sampling of smaller microspheres and lower forces. Our linearized model, however, does not allow correct determination of forces that lie in the entropic regime (<0.1 pN) (Fig. 3 *c*, *black points* and *blue line*). At these low forces, the force can be calibrated accurately by determining the RMS displacement of the microspheres (see the Supporting Material) and comparing that with simulated data using the full kinetic model based on Eqs. 1 and 2 (Fig. 3 *c*, *red dots*). Note that RMS displacement determination is the key detection method in TPM experiments (15). Using this approach, OP forces were determined accurately for 440-nm-diameter microspheres to

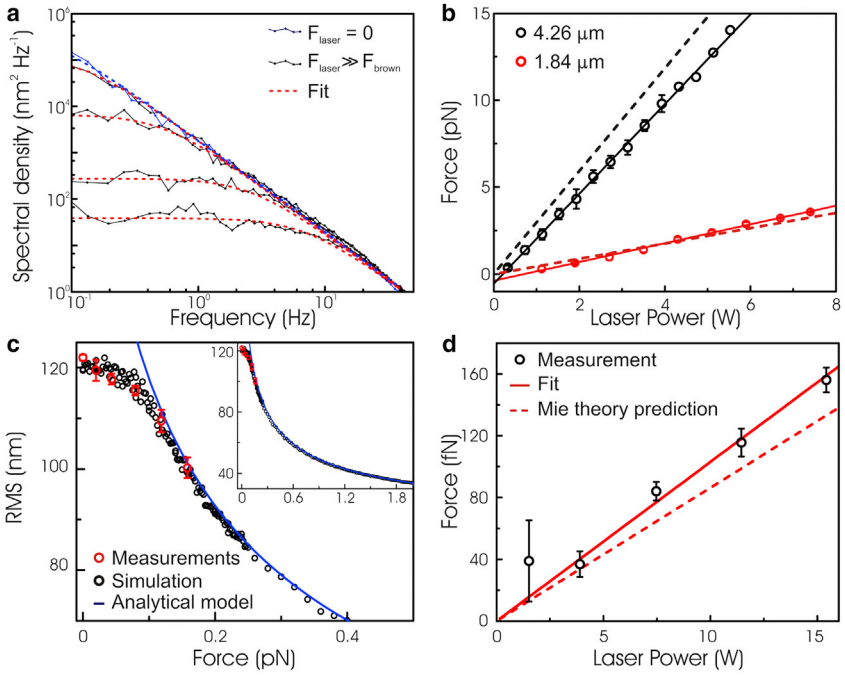

FIGURE 3 (*a*) Fitted power spectra of the measured *x*,*y* motion of 4.26-μm tethered microspheres. A power spectrum obtained in the absence of force is shown for reference. The other spectra from top to bottom are obtained using laser powers of 0.2 W (0.3 $\pm$ 0.1 pN), 0.7 W (1.0 $\pm$ 0.2 pN), 2.7 W (5.2 $\pm$ 0.3 pN), and 6.2 W (12.7 $\pm$ 0.8 pN). (*b*) Exerted optical pushing force as a function of total laser intensity at the sample. Forces are determined by fitting the power spectra of measured polystyrene tethers with the analytical theory (*error bars*, mean $\pm$ SE). (*Solid lines*) Linear fits yielding slopes of 2.6 $\pm$ 0.1 pN W^{-1} and 0.5 $\pm$ 0.1 pN W^{-1}. (*c*) RMS motion of small (ϕ 440 nm) microspheres for measured, simulated, and calculated data using our analytical model (Eq. 3). (*d*) The derived force, using the RMS fitted data sets, as a function of laser power applied. The linear fit yielded a slope of 10.6 fN/W (see the Supporting Material).

be 10.6 fN/W at the sample (Fig. 3 *d*), again in agreement with Mie theory.

Manipulating protein looped DNA

To demonstrate the power of OP in bionano-technological applications, we performed a force-spectroscopy study of protein-induced DNA looping. Looping is often studied with TPM setups because of their ability to detect looping at very low forces. DNA loops occur whenever proteins interact with multiple sites on the same DNA molecule (17). Loops have both organizing and regulatory functions in processes such as DNA replication, repair, transcription, and cleavage (18,19). We chose Type-II restriction endonuclease *Fok*I as our model system, because *Fok*I has been well studied by biochemical and biophysical (TPM) means (20–22). Two *Fok*I monomers each bind to distinct recognition sites on the DNA (5-GGATG-3); subsequently, they associate in dimers while both monomers remain attached to the DNA, forming a DNA loop (20). When only Ca^{2+} (and not Mg^{2+}) is present in solution as a cofactor, the restriction enzymes specifically bind to the DNA, forming loops, but they cannot cut the DNA (23,24). Looping of multiple DNA molecules with a contour length of 184 nm containing two *Fok*I recognition sites (spaced 65 nm apart) was monitored in real-time using our OP microscope. Excursions of DNA-tethered microspheres depend on the length of the DNA and, as a consequence, loop formation can be observed as a decrease in the microspheres' RMS motion. In this study we only analyzed the transition from looped to unlooped state, which occurs in a single kinetic step. The opposite transition, from unlooped to looped state, consists of two distinct, subsequent kinetic steps, one of which depends on protein concentration and tether activity, and is therefore far more complex to interpret (see Fig. 4 *a*) (21).

Example OP time traces of the RMS displacement in the presence of *Fok*I are shown in Fig. 4 *b*. The RMS motion of each microsphere was calculated as described by Laurens et al. (21). When the laser is off, the system stochastically switched between the unlooped and looped state. With increasing laser intensity, and thus increased force applied to the DNA tether, loop formation was less frequent (Fig. 4 *b*) and loops lasted for shorter times (Fig. 4 *c*). Measurements on multiple microspheres simultaneously enhanced experimental throughput (see Fig. S6) and allowed obtaining the force dependence of the average loop lifetime t_{loop} (Fig. 4 *c*). This lifetime decayed exponentially with force, as expected from Arrhenius' law $t_{\mathrm{loop}} = 1/k_0 \exp(-F_{\mathrm{laser}} \times \Delta x/k_{\mathrm{B}}T)$ (with k_0 being the unlooping rate at zero force, and Δx as the distance to the barrier along the direction at which the force F_{laser} is applied). The expected heating near the sample is $<$3 K for the used laser power, hence the temperature change should hardly affect the kinetics of the reaction (see the Supporting Material). The single-exponential decay indicates that the transition from looped to unlooped state involves a single kinetic step. From the fit, a zero-force unlooping rate (k_0) of 0.15 $\pm$ 0.01 s^{-1} was obtained, in agreement with earlier measurements (21). In addition, a length change from looped state to transition state (Δx) of 75 $\pm$ 2 nm was obtained. This length change is relatively large because it

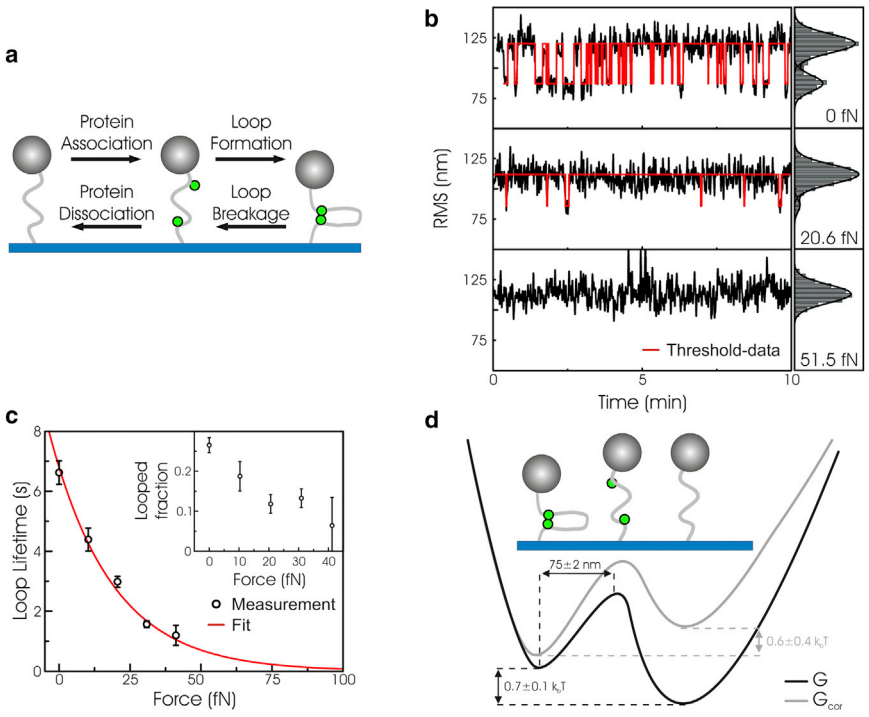

FIGURE 4 (*a*) Kinetic scheme of protein-induced DNA looping. (*b*) Time traces of the RMS motion of a single DNA tether (*left panel*, *black line*) calculated over a 2 s time-window, and the corresponding histograms (*right panel*), with increasing optical pushing force. The histograms show two distinct states corresponding to the unlooped (large RMS) and looped state (small RMS). From the histograms a threshold value is obtained, which is used to determine the dwell times (*red lines*, *left panels*). (*c*) Average loop lifetime plotted as a function of optical pushing force. (*Black circles*) Experimental data points (*error bars*, mean ± SE); (*red line*) fit using Arrhenius' law; (*inset*) looped fraction as a function of the optical pushing force (*error bars*, mean ± SE). (*d*) Energy landscape obtained from the force spectroscopy measurements. The corrected free energy G_{cor} takes the volume exclusion force into account due to the close proximity of the surface.

exceeds the size of the protein by at least one order of magnitude, which demonstrates that only very small forces, in the femtoNewton range, are required to disrupt the DNA looping. At these low forces, the DNA is in a coiled conformation and therefore the elasticity of the DNA contributes significantly to Δx, because force is applied to the protein complex via two elastic DNA linkers. Because the volume-exclusion effect is of the same order of magnitude as the protein-protein bond strength, it is important to correct the unlooping rate at zero force for this volume-exclusion effect, which, in turn, is dependent on the size of the microspheres and the interactions with the surface. In our setup, the volume-exclusion effect generates an effective force on the DNA of ~52 fN in the looped state (25). Under the assumption that the volume-exclusion force acts as a constant force offset (see Fig. S7), correction reduces the unlooping rate by a factor of 10, $k_{0,cor} = 0.015 \pm 0.003\ s^{-1}$. Apart from the looping rate, the looped fraction was also obtained from the data, which allowed calculation of the force dependence of the free energy change from the unlooped to the looped state (see Fig. S8). This approach yielded a standard free energy change ΔG^0 of $0.7 \pm 0.1\ k_BT$ (with the unlooped state having a lower free energy). However, this ΔG^0 needs to be corrected because the volume-exclusion effect introduces an energy penalty for looping to occur. When we correct for this, it yields a ΔG^0_{corr} of $-0.6 \pm 0.4\ k_BT$ ($G^0_{loop,cor} - G^0_{unloop,cor}$), i.e., leading to the expected situation in which the looped state has a lower free energy. The low forces that are needed to disrupt the protein-induced DNA loops indicate that thermal fluctuations are sufficient to cross the energy barrier from looped to unlooped state and vice versa, which from a biological point of view makes sense because restriction enzyme function is to recognize and cut specific sequences within a few seconds and not to mechanically stabilize DNA loops for longer time periods (21). This determination of energetics and kinetics of the *Fok*I restriction enzyme demonstrates the great level of control OP provides in the femtoNewton force regime, allowing the extraction of subtleties in the energy landscapes of molecular interactions as well as the characterization of the impact of surfaces on bond formation (see Fig. 4 *d*).

DISCUSSION

We have characterized the performance of our novel, to our knowledge, OP method and shown its potential by unraveling the energy landscape of the DNA-looping *Fok*I restriction enzyme by the use of constant force measurements. Apart from applying a constant force, OP is capable of rapidly switching and changing forces, by shuttering or strobing the incoming light, or varying the intensity using, for example, an acousto-optical modulator. This allows OP to apply a wide dynamic range of loading rates, as is required for dynamic force spectroscopy (4). Radiation pressure travels at the speed of light, the theoretical response time of a typical DNA-tethered microsphere is, however, limited by viscous drag (slowing down the motion of the microsphere and thus the extension of the loading of the tether) to typically ~100 μs (see the Supporting Material).

From this, we estimate that OP can be used to apply linear force ramps in the range of 10^{-4} to 10^{6} pN/s to DNA (see Fig. S9). Today's MT systems allow access to a more limited range of loading rates from 10^{-4} to 10^{2} pN/s (26).

It should be noted that one does need to take care of sample and instrument heating caused by the high laser powers used. We were able to reduce heating effects by using quartz microscope slides and coverslips. We estimate that the heating in the center of the flow cell is ~0.7 K/W (see calculations in the Supporting Material). Note that the coverslip acts as an effective heat sink, which substantially reduces the effect of heating near the glass surface (27) where our assay is mostly located, and thus the 0.7 K/W heating represents an upper limit. Although the laser power used in OP is typically an order-of-magnitude higher than in optical tweezers, the laser intensity is approximately three orders-of-magnitude lower, because the laser beam is not focused. The heating of the instrument is mostly due to light absorption in the objective. The subsequent warming of the objective causes slow but considerable drift in the instrument. Currently, it limits the force range that can be reliably be sampled to several picoNewtons.

To calibrate the forces in OP, we derived an analytical description of the power spectrum, taking into account Brownian rotation of the tethered microspheres (Eq. 3). We note that our equation can be used more generally for tethered systems (including MTs) as long as the externally applied force on the microsphere dominates the Brownian force, i.e., $F_{\text{ext}} >> F_{\text{brown}}$. Fig. S3 shows how the analytical power spectrum derived here compares to the MT power spectrum used by te Velthuis et al. (11) for the dimension perpendicular to the direction of the field lines as

$$P(f) = \frac{2\gamma k_{\text{B}}T}{\gamma^2(2\pi f)^2 + \left(F_{\text{ext}}/(L_{\text{ext}}+R)\right)^2}, \qquad (4)$$

with L_{ext} as the DNA extension. The MT model only holds for microspheres with diameters smaller than the contour length of the DNA (Fig. S10 *c*); for larger microspheres, the MT model underestimates the Brownian motion of the microsphere (Figs. S10 *a* and S9 *b*). In contrast, our model was able to describe the Brownian motion for the larger microspheres; it fails, however, for external forces lower than the Brownian force (<0.1 pN). We have shown that the Brownian motion can be predicted accurately in this low-force regime (down to ~30 fNs) with numerical simulations. By making use of the analytical solution (Eq. 3) for the enthalpic regime (>0.1 pN) and the numerical simulations in the entropic regime (<0.1 pN), we were able to predict microsphere motion subjected to forces that are biophysically relevant. Due to its generality, applicability of our model is not constrained to OP alone—it is also applicable to microsphere-tether systems such as MTs and TPM.

We have shown that a collimated laser beam can be used to apply a force to multiple biomolecules in parallel (Fig. S6). We have demonstrated the feasibility of OP as a flexible (dynamic) force spectroscopy technique. In future implementations, improvements can be made, inspired by other force-spectroscopy approaches. For example, spatial light modulators (21,28) could be used to flatten the light intensity; the number of usable tethers could be increased by printing antibodies in a periodic pattern on a coverslip (29); (sub)millisecond dynamics of weak DNA-enzyme interactions could be imaged using integrated fluorescence microscopy (29,30); or the polarization of the laser light could be employed to control the torque acting on the biomolecules (31,32). Finally, OP instruments can be readily implemented in any existing OTs instrument: placing a single lens, by converting a collimated beam in one focused in the back-focal plane of the microscope objective, will convert an OTs into an OP apparatus.

SUPPORTING MATERIAL

Supporting Materials and Methods, eleven figures, and one table are available at http://www.biophysj.org/biophysj/supplemental/S0006-3495(15)01211-4.

AUTHOR CONTRIBUTIONS

The article was written with the contributions of all authors. All authors gave their approval to the final version of the article.

ACKNOWLEDGMENTS

This work is part of the research program of the Foundation for Fundamental Research on Matter (to E.J.G.P. and G.J.L.W.), which is part of the Netherlands Organization for Scientific Research. We acknowledge support by the Netherlands Organization for Scientific Research, VICI grant (to E.J.G.P. and G.J.L.W.), as well as a European Research Council starting grant (to G.J.L.W.).

REFERENCES

1. Gellert, M., and H. Nash. 1987. Communication between segments of DNA during site-specific recombination. *Nature.* 325:401–404.
2. Smith, S., L. Finzi, and C. Bustamante. 1992. Direct mechanical measurements of the elasticity of single DNA molecules by using magnetic beads. *Science.* 258:1122–1126.
3. Ashkin, A. 1992. Forces of a single-beam gradient laser trap on a dielectric sphere in the ray optics regime. *Biophys. J.* 61:569–582.
4. Merkel, R., P. Nassoy, …, E. Evans. 1999. Energy landscapes of receptor-ligand bonds explored with dynamic force spectroscopy. *Nature.* 397:50–53.
5. Halvorsen, K., and W. P. Wong. 2010. Massively parallel single-molecule manipulation using centrifugal force. *Biophys. J.* 98:L53–L55.
6. Binnig, G., C. F. Quate, and C. Gerber. 1986. Atomic force microscope. *Phys. Rev. Lett.* 56:930–933.
7. Svoboda, K., C. F. Schmidt, …, S. M. Block. 1993. Direct observation of kinesin stepping by optical trapping interferometry. *Nature.* 365:721–727.

8. Neuman, K. C., and A. Nagy. 2008. Single-molecule force spectroscopy: optical tweezers, magnetic tweezers and atomic force microscopy. *Nat. Methods.* 5:491–505.
9. Laurens, N., S. R. W. Bellamy, …, G. J. Wuite. 2009. Dissecting protein-induced DNA looping dynamics in real time. *Nucleic Acids Res.* 37:5454–5464.
10. Strick, T. R., J. Allemand, …, V. Croquette. 1996. The elasticity of a single supercoiled DNA molecule. *Science.* 271:1835–1837.
11. te Velthuis, A. J. W., J. W. J. Kerssemakers, …, N. H. Dekker. 2010. Quantitative guidelines for force calibration through spectral analysis of magnetic tweezers data. *Biophys. J.* 99:1292–1302.
12. Reif, F. 1985. Fundamentals of Statistical and Thermal Physics. McGraw-Hill, Singapore.
13. Howard, J. 2001. Mechanics of Motor Proteins and the Cytoskeleton. Sinauer, Sunderland, MA.
14. Daldrop, P., H. Brutzer, …, R. Seidel. 2015. Extending the range for force calibration in magnetic tweezers. *Biophys. J.* 108:2550–2561.
15. Han, L., B. Lui, …, R. Phillips. 2009. Chapter 150. *In* Calibration of Tethered Particle Motion Experiments. C. J. Benham, S. K. Harvey, W. K. Olson, D. W. L. Sumners, and D. Swigon, editors. Springer, New York, pp. 123–138.
16. C. F. Bohren, and D. R. Huffman, editors 1998. Absorption and Scattering of Light by Small Particles. Wiley-VCH, Weinheim, Germany.
17. Saiz, L., and J. M. G. Vilar. 2006. DNA looping: the consequences and its control. *Curr. Opin. Struct. Biol.* 16:344–350.
18. Allen, D. J., A. Makhov, …, J. D. Griffith. 1997. MutS mediates heteroduplex loop formation by a translocation mechanism. *EMBO J.* 16:4467–4476.
19. Halford, S. E., A. J. Welsh, and M. D. Szczelkun. 2004. Enzyme-mediated DNA looping. *Annu. Rev. Biophys. Biomol. Struct.* 33:1–24.
20. Bitinaite, J., D. A. Wah, …, I. Schildkraut. 1998. *Fok*I dimerization is required for DNA cleavage. *Proc. Natl. Acad. Sci. USA.* 95:10570–10575.
21. Laurens, N., D. A. Rusling, …, G. J. L. Wuite. 2012. DNA looping by *Fok*I: the impact of twisting and bending rigidity on protein-induced looping dynamics. *Nucl. Acids Res.* 40:4988–4997.
22. Rusling, D., A. N. Laurens, …, S. E. Halford. 2012. DNA looping by *Fok*I: the impact of synapse geometry on loop topology at varied site orientations. *Nucleic Acids Res.* 40:4977–4987.
23. Vipond, I. B., and S. E. Halford. 1995. Specific DNA recognition by *Eco*RV restriction endonuclease induced by calcium ions. *Biochemistry.* 34:1113–1119.
24. Embleton, M. L., S. A. Williams, …, S. E. Halford. 1999. Specificity from the synapsis of DNA elements by the *Sfi*I endonuclease. *J. Mol. Biol.* 289:785–797.
25. Segall, D. E., P. C. Nelson, and R. Phillips. 2006. Volume-exclusion effects in tethered-particle experiments: bead size matters. *Phys. Rev. Lett.* 96:088306.
26. Yang, Y., R. M. Erb, …, B. B. Yellen. 2011. Imaginary magnetic tweezers for massively parallel surface adhesion spectroscopy. *Nano Lett.* 11:1681–1684.
27. Peterman, E. J. G., F. Gittes, and C. F. Schmidt. 2003. Laser-induced heating in optical traps. *Biophys. J.* 84:1308–1316.
28. Kress, H., J.-G. Park, …, E. R. Dufresne. 2009. Cell stimulation with optically manipulated microsources. *Nat. Methods.* 6:905–909.
29. De Vlaminck, I., and C. Dekker. 2012. Recent advances in magnetic tweezers. *Annu. Rev. Biophys.* 41:453–472.
30. Gross, P., G. Farge, …, G. J. Wuite. 2010. Combining optical tweezers, single-molecule fluorescence microscopy, and microfluidics for studies of DNA-protein interactions. *Methods Enzymol.* 475:427–453.
31. La Porta, A., and M. D. Wang. 2004. Optical torque wrench: angular trapping, rotation, and torque detection of quartz microparticles. *Phys. Rev. Lett.* 92:190801.
32. Pedaci, F., Z. Huang, …, N. H. Dekker. 2010. Excitable particles in an optical torque wrench. *Nat. Phys.* 7:259–264.

Optical Pushing: A tool for parallelized biomolecule manipulation

Gerrit Sitters[‡1], *Niels Laurens*[‡1*], *Emile J de Rijk*[1,], *Holger Kress*[2,3], *Erwin JG Peterman*[1], *Gijs JL Wuite1*[1,*]

1. Department of Physics and Astronomy and Laser Centre, VU University, The Netherlands

2. Experimental Physics I, University of Bayreuth, Bayreuth, Germany

3. Department of Applied Physics, Eindhoven University of Technology, Eindhoven, The Netherlands

Supplementary information

Proteins and buffers. The FokI protein was purified was purified from an over-producing strain of E-coli. DNA binding experiments were performed in a 20mM Tris-acetatie (pH 7.8), 50 mM potassium acetate, 2 mM $CaCl_2$ and I mM DTT buffer. Experiments on naked DNA were conducted in PBS.

The analytical model. To determine the exerted force on tethered molecules it is important to understand the motion of the system. Apart from translational Brownian motion the microspheres also experiences rotational Brownian motion causing them to swivel around the attachment point as shown schematically for one dimension in **Supplementary Fig. 2a,b**. Existing force calibration methods for tethered microspheres, which are used for instance for MT, are not directly applicable to our system. Microsphere rotation is neglected in these models because of the fixed alignment of the paramagnetic microsphere with the external magnetic field[1]. Neglected microsphere rotation leads to an underestimation of the applied force (**Supplementary Fig. 3**). We therefore derived a power spectrum for the microspheres motion parallel to the surface using the Langevin equation for both the translation as the rotation[2,3]:

$$m\frac{d\vec{v}}{dt} = \vec{F}_{brown}(t) - \vec{\gamma}\cdot\vec{v}(t) + \vec{F}_{ext}(t)$$
$$I\frac{d\vec{\omega}}{dt} = \vec{T}_{brown}(t) - \vec{\beta}\cdot\vec{\omega}(t) + \vec{T}_{ext}(t)\,, \qquad (5)$$

where $\vec{v}$ and $\vec{\omega}$ are respectively the translational and angular velocity, m is the particle mass and I is the moment of inertia of the particle. The forces due to the laser, the tether, the surface, buoyancy and

gravity are included in the external force term $\vec{F}_{ext}$ and are described in detail bellow. Equations (5) account for the increased viscous drag near the surface, using Faxen's law for both the translation and rotation coefficients $\vec{\gamma}$ and $\vec{\beta}$ (see section surface effects, equations (12)). The external torque $\vec{T}_{ext}$ results from the cross product of the vector between the microsphere center and the DNA attachment point $\vec{R}$ and the DNA force $\vec{F}_{DNA}$ (**Supplementary Fig. 2b**). $\vec{F}_{brown}$ and $\vec{T}_{brown}$ are the fluctuating thermal force and torque. The amplitude of these terms are described by the fluctuation-dissipation theorem and are Gaussian distributed with the following statistical properties[4]:

$$\langle F_{brown}(t)\rangle = 0$$
$$\langle T_{brown}(t)\rangle = 0$$

$$\langle F_{brown}(t')F_{brown}(t'+t)\rangle = 2\gamma k_B T\delta(t)$$

$$\langle T_{brown}(t')T_{brown}(t'+t)\rangle = 2\beta k_B T\delta(t). \qquad (6)$$

With $\delta(t)$ the Dirac delta function. The inertial terms in equations .5) are neglected since the Reynolds number is sufficiently low. For microspheres in the micro range the Reynolds number is in the order of $1\cdot 10^{-3}$ at room temperature (**Supplementary Table 1**).

To simplify calculations we assume a laser force $F_{laser} \gg F_{brown}$, leading to small angles of θ, α, φ, β and ξ (**Supplementary Fig. 2a,b**). The DNA-microsphere system is in equilibrium when the DNA and vector $\vec{R}$ are aligned with the z axis. If the system is pulled out of equilibrium due to Brownian fluctuations the DNA and the laser force will tend to force the microsphere back into equilibrium:

$$F_{restoring,x} = F_{DNA}\cdot sin\theta$$

$$T_{restoring,y} = |R|\cdot|F_{DNA}|\cdot sin\beta. \qquad (7)$$

Assuming that $|F_{DNA}| = |F_{laser}|$ (for $\theta \ll 1$), $|\varphi| + \alpha + \xi \ll 1$ and $x_{cm} = x_{DNA} + R\varphi$ (see **Supplementary Figure 2a,b** we derive the following linearized versions of equations (7):

$$\beta = \pi - (\alpha+\varphi) - \xi$$

$$\alpha = \tan^{-1}\frac{x_{cm}}{z} \approx \frac{x_{cm}}{z}$$

$$(z-R)\,\xi \approx R(\alpha+\varphi) \rightarrow \xi \approx \frac{R\alpha}{z-R} + \frac{R|\varphi|}{z-R} \approx \frac{Rx_{cm}}{z^2-zR} + \frac{R|\varphi|}{z-R}$$

$$F_{restoring,x} = F_{laser}\cdot\frac{x_{DNA}}{z-R} = F_{laser}\cdot\frac{x_c - R\varphi}{z-R}$$

$$T_{restoring} = |R|\cdot|F_{laser}|\cdot sin(\pi - |\varphi| - \alpha - \xi) = |R|\cdot|F_{laser}|\cdot sin(|\varphi| + \alpha + \xi)$$
$$= |R|\cdot|F_{laser}|\cdot\left(|\varphi| + \frac{x_{cm}}{z} + \frac{Rx_{cm}}{z^2-zR} + \frac{R|\varphi|}{z-R}\right). \qquad (8)$$

See **Supplementary Figure 2c** how they compare to the non-linearized force and torque (using the numerical simulations described below). To calculate the power spectrum of equations (5) we

implement the linearized restoring force and torque as the external force and torque in these equations and calculate the Fourier transform, with $\tilde{x}(\omega) = \int_{-\infty}^{\infty} x(t)e^{-i\omega t}dt$. Note that surface, buoyancy and gravity forces are neglected:

$$\tilde{F}_{brown} = i\omega\gamma\tilde{x}_{cm} - \frac{F_{laser}}{z-R}(\tilde{x}_{cm} - R\tilde{\varphi})$$

$$\tilde{T}_{brown} = i\omega\beta\tilde{\varphi} - RF_{laser}\left(|\tilde{\varphi}| + \frac{\tilde{x}_{cm}}{z} + \frac{R\tilde{x}_{cm}}{z^2-zR} + \frac{R|\widetilde{\varphi}|}{z-R}\right). \quad (9)$$

From these equations we derive the power spectrum $P(f) \equiv \langle\tilde{x}_{cm}\tilde{x}_{cm}^*\rangle$, with the frequency f (* denotes the complex conjugate), using the relations $\langle\tilde{F}_{brown}^2\rangle = 2\gamma k_B T$ and $\langle\tilde{T}_{brown}^2\rangle = 2\beta k_B T$:

$$P(f) = 2k_b T\frac{(\beta+\gamma\langle z\rangle^2)R^2F^2+(\langle z\rangle-R)^2\beta^2\gamma(2\pi f)^2}{\left((R-\langle z\rangle)\beta\gamma(2\pi f)^2+RF^2\right)^2+(2(R\gamma\langle z\rangle-\beta)F\pi f)^2}. \quad (10)$$

Note that the equation (10) reduces to the power spectrum of magnetic tweezers when $\beta = 0$ (neglecting rotation) is implemented (equation 4).

Numerical simulations. To validate the assumptions made in the derivation of the analytical power spectrum we also simulated microsphere movement. The microsphere equation of translation and rotation was solved numerically using the following equations:

$$\vec{x}_{n+1} = \vec{x}_n + \vec{\gamma}^{-1}\cdot\left(\vec{F}_{ext} + \vec{F}_{brown}\right)\Delta t$$

$$\vec{\varphi}_{n+1} = \vec{\varphi}_n + \vec{\beta}^{-1}\cdot\left(\vec{T}_{ext} + \vec{T}_{brown}\right)\Delta t, \quad (11)$$

where $\vec{x}_n$ and $\vec{x}_{n+1}$ is the microspheres three dimensional position at the step n and $n+1$ of the simulation respectively. $\vec{\varphi}_n$ and $\vec{\varphi}_{n+1}$ denote the microspheres orientation. In order to simulate the microspheres trajectory we implemented an initial microsphere position and rotation, after which successive positions and rotations were calculated using equations (11). The Brownian force and torque terms were drawn from Gaussian distributions that suffice equations (6) where the Dirac delta distribution was set to $\delta(t) = 1/\Delta t$, with Δt the time step of the simulation for which we typically used 10^{-5}s. Decreasing Δt did not affect the statistical properties (such as the RMS, correlation time and power spectra) of the simulated traces.

Surface effects. Equations (5) account for the increased viscous drag near the surface, using Faxen's law for both the translation and rotation coefficients for the parallel and perpendicular direction relative to the surface[5]:

$$\gamma_x = \gamma_y = \frac{\gamma_0}{1 - \frac{9}{16}\left(\frac{R}{z}\right) + \frac{1}{8}\left(\frac{R}{z}\right)^3 - \frac{45}{256}\left(\frac{R}{z}\right)^4 - \frac{1}{16}\left(\frac{R}{z}\right)^5}$$

$$\gamma_z = \frac{\gamma_0}{1 - \frac{9}{8}\left(\frac{R}{z}\right) + \frac{1}{2}\left(\frac{R}{z}\right)^3 - \frac{57}{100}\left(\frac{R}{z}\right)^4 + \frac{1}{5}\left(\frac{R}{z}\right)^5 + \frac{7}{200}\left(\frac{R}{z}\right)^{11} - \frac{1}{25}\left(\frac{R}{z}\right)^{12}}$$

$$\beta_x = \beta_y = \frac{\beta_0}{1 - \frac{1}{8}\left(\frac{R}{z}\right)^3}$$

$$\beta_z = \frac{\beta_0}{1 - \frac{5}{16}\left(\frac{R}{z}\right)^3 + \frac{15}{256}\left(\frac{R}{z}\right)^6} \quad (12)$$

where γ_0 and β_0 are respectively the translational and rotational drag coefficients in bulk and are defined as $\gamma_0 = 6\pi\eta R$ and $\beta_0 = 8\pi\eta R^3$, with R is the microspheres radius and z is the microsphere center-surface separation in the axial direction and η representing the dynamic viscosity.

External forces. The external forces that are implemented in our numerical simulation are the laser force $\vec{F}_{laser}$, the force of the DNA $\vec{F}_{DNA}$, the force of the surface $\vec{F}_{surface}$, the buoyancy force $\vec{F}_{buoyancy}$ and the gravitational force $\vec{F}_{gravity}$. The laser force is implemented as a constant force in z direction and is set manually:

$$\vec{F}_{laser} = F_{laser}\hat{z} \quad (13)$$

The force of the DNA is calculated with the extensible worm like chain model[6]:

$$\vec{F}_{DNA} = -\left(\frac{k_B T}{L_p}\right)\left[\frac{1}{4}\left(1 - \frac{\vec{a}}{L_c} + \frac{\vec{F}_{DNA}}{S}\right)^{-2} - \frac{1}{4} + \frac{\vec{a}}{L_c} - \frac{\vec{F}_{DNA}}{S}\right], \quad (14)$$

with L_p, L_c and S respectively the persistence length, the contour length and the stretch modules of DNA (**Supplementary Table 1**). The vector $\vec{a} = (x_{DNA}, y_{DNA}, z_{DNA})$ points from the DNA-surface attachment point towards the DNA-microsphere attachment point. The surface force results from the electrostatic interaction between microsphere and surface[7]:

$$\vec{F}_{surface} = 4\pi\epsilon_W\epsilon_0\psi_0^2 R e^{-(z-R)/l}\hat{z}\,, \quad (15)$$

with ϵ_W and ϵ_0 respectively the permittivity of water and vacuum, ψ_0 the effective surface potential, R the microsphere radius, z the axial distance between surface and microsphere center and l the Debye screening length. The buoyancy and gravity forces are implemented as follows:

$$\vec{F}_{buoyancy} + \vec{F}_{gravity} = \frac{4}{3}\pi R^3 g(\rho_{med} - \rho_{bead})\hat{z}, \quad (16)$$

with g the gravitational constant, ρ_{med} the density of water and ρ_{bead} the density of the microsphere. See the supplementary information for the parameters used.

Mie calculations. Radiation pressure exerted on a spherical particle by a beam of light is calculated using Mie theory[8]. The laser force is expressed in terms of the extinction coefficient C_{ext}, the scattering cross section C_{sca} and the average cosine of the scattering angles $\langle cos\theta \rangle$:

$$F_{laser} = \frac{n_m I}{c}(C_{ext} - C_{sca}\langle cos\theta \rangle), \quad (17)$$

with n_m the refractive index of the surrounding medium, I the laser intensity and c the speed of light. C_{ext}, C_{sca} and $\langle cos\theta \rangle$ are expressed by:

$$C_{sca} = \frac{2}{x^2}\sum_{n=1}^{\infty}(2n+1)(|a_n|^2 + |b_n|^2),$$

$$C_{ext} = \frac{2}{x^2}\sum_{n=1}^{\infty}(2n+1)Re\{a_n + b_n\},$$

$$\langle cos\theta \rangle = \frac{4\pi R^2}{x^2 C_{sca}}\sum_{n=1}^{\infty}\left[\frac{n(n+2)}{n+1}Re\{a_n a_{n+1}^* + b_n b_{n+1}^*\} + \frac{2n+1}{n(n+1)}Re\{a_n b_n^*\}\right], \quad (18)$$

where $x = 2\pi R/\lambda$, R is the particle radius, λ is the wavelength of the light in the surrounding medium and the asterisk denotes complex conjugation. a_n and $b_n$are classical Mie coefficients depending on the particle size and material. The calculation of these coefficients is done according to Bohren et al[8]. See the **Supplementary Table 1** for the material parameters.

Once a_n and b_n are calculated the equation above are used to derive the laser force acting on the particles numerically. To decrease computation times, the summations are terminated after $n_{max=}x + 4x^{1/3} + 2$. This amount a terms has proven to be sufficient to calculate a_n and b_n correctly[8].

Loading rates. Laser powers and therefore the laser forces on the microspheres can be altered with a frequency in the 100Mhz regime using AOMs. The tension of the DNA will respond much slower due to the viscous drag of the microsphere. To calculate the response time of the system the following equation of motion for the microsphere is solved (inertia is neglected):

$$F_{laser}(t) - \gamma\dot{x}(t) - kx(t) = 0, \quad (19)$$

with $\dot{x}$ the time derivative of the position x and k the stiffness of the DNA. If we assume that both the laser force and the stiffness of the DNA are constant, the solution of the equation of motion is $(t) = \frac{F_{laser}}{k}\left(1 - e^{-\frac{k}{\gamma}t}\right)$. The response time of the system is thus proportional to $\frac{\gamma}{k}$. **Supplementary Figure 7a** shows that the typical switching time lies in the order of 100 µs for 4µm microsphere in diameter and a DNA stiffness of 2,000 $pN/\mu m$ (enthalpic regime of DNA with L_c=0.5 µm). Linear force ramps exerted on the DNA can be achieved below the response time of the system if a linearly increasing laser force is applied with an initial offset (**Supplementary Fig. 7b**). The initial laser offset that should be applied to create a linear loading rate on the DNA is proportional to the height of the loading rate. This limits the force range for high loading rates. **Supplementary Figure 7b** shows that it is possible to apply a loading rate of $10^6\ pN\ /\ s$ over 50 % of the total force range. This range increases to 95 % for a loading rate of $10^5\ pN\ /\ s$. The smallest achievable loading rate using OP is limited by the laser power stability, which typically fluctuates 1 % over 4 hours (IPG laser spec. sheet). To achieve a loading rate that is linear within an accuracy of 10 %, the loading rate should at least be ten times larger than the rate of the laser power fluctuations. This results in a minimal loading rate of $\frac{F_{laser,max}}{1440s} \sim 3 \cdot 10^{-2}\ pN\ /\ s$ for a maximum loading force of 40 pN. The power fluctuations of the laser can be reduced using a feedback loop to control the laser power. Laser intensity stabilizers can attenuate the noise by a factor

of 400.[9] This decreases the minimum force ramp to $\sim 1 \cdot 10^{-4}\ pN\ /\ s$ for a maximum loading force of 40 pN.

Force calibration using RMS motion. To calibrate the forces on the small beads (ϕ 440 nm) in the entropic regime (<0.1 pN) we used our numerical simulations (see Figure 3c). To determine the calibration factor we calculated the root mean square difference ($RMSD = \sqrt{\frac{\sum_N (RMS_{meas} - RMS_{sim})^2}{N}}$) between the simulated and measured data points as a function of calibration factor (see Supplementary Figure 11)

Sample heating. Since a high intensity laser is used to apply forces in the sample, it is important to quantify any potentially harmful heating effects. It has been shown that in an optical tweezers experiment, where the light ($100\mathrm{mW}$ at $1064\mathrm{nm}$) is tightly focused, there is a small temperature increase of approximately 0.8 K in the focus, which does not damage the biological sample[10]. The laser powers used in the Optical Pushing instrument is two orders of magnitude higher (up to 15W), but the laser beam is not focused in the sample. Therefore it is of interest to calculate the heating, using the theoretical model that is derived by Peterman et al. [10] and applying it to a collimated beam.

Laser induced heating is mainly determined by the heating of the buffer in the sample and has a maximum in the center of the flow cell. A solvent's ability to absorb a plane wave of light with intensity I travelling in the x-direction through the solvent is determined by its extinction coefficient γ, which is translated to the heat per volume, Q, generated per time in the solvent:

$$I(x) = I_0 e^{-\gamma x}, \tag{19}$$

$$\frac{dQ}{dt} = -\frac{dI}{dx} = \gamma I\ . \tag{20}$$

This generated heat will be dissipated by a heat flow J that is calculated using the local differential equation:

$$J\left(\vec{r}\right) = -C\nabla\left(\Delta T\left(\vec{r}\right)\right), \tag{21}$$

where C is the thermal conductivity of the solvent and $\Delta T(\vec{r})$ is the temperature deviation from ambient temperature due to heating at position $\vec{r}$. In a steady state solution the heat generated is in equilibrium with the amount of heat dissipated: $\nabla J = dQ/dt$, leading to (using equations (20) and(21)):

$$\nabla^2\left(\Delta T\left(\vec{r}\right)\right) = -\frac{\gamma}{C} I\left(\vec{r}\right). \tag{22}$$

Solving equation 22 for $r = 0$ will give the temperature increase in the center of the laser beam. To solve equation 22 the Green's function is used that satisfies:

$$\nabla^2 G\left(\vec{r}, \vec{r}\,'\right) = \delta^3\left(\vec{r}, \vec{r}\,'\right), \tag{23}$$

with δ the Dirac delta function. Setting the argument $\vec{r}'$ to zero and implementing the boundary condition of $G = 0$ at a radial distance S leads to:

$$G(r) = -\frac{1}{4\pi}\left(\frac{1}{r} - \frac{1}{S}\right). \tag{24}$$

This boundary condition represents the quartz surface that is present at a distance S and acts as a heat sink. To calculate the maximum temperature in the center of the flow cell, an S of $50\ \mu\mathrm{m}$ is taken into account. In terms of $G(r)$, the solution of equation (22) at the center of the laser beam is:

$$\Delta T(0) = \int G(r)\left(-\frac{\gamma}{C} I(r)\right) dV\ . \tag{25}$$

Setting $dV = r^2 dr d\Omega$ and implementing $G(r)$ and $I(r)$, leads to:

$$\Delta T = \frac{\gamma I_{tot}}{8\pi^2 C\beta^2} \int_{r<R} \left(\frac{1}{r} - \frac{1}{S}\right) e^{\frac{-r^2}{2\beta^2}} r^2 dr d\Omega \quad = \quad \frac{\gamma I_{tot}}{4\pi C\beta^2} \int_0^R \left(\frac{1}{r} - \frac{1}{S}\right) e^{\frac{-r^2}{2\beta^2}} r^2 dr\ , \tag{26}$$

where I_{tot} is the total laser intensity and $\beta = FWHM/2\sqrt{2ln2}$. This integral is solved numerically, which results in a heating of approximately $0.72\ \mathrm{K}$ at the center of the flow chamber when the following parameters are implemented: $\alpha = 14.2\mathrm{m}^{-1}$ (extinction coefficient of water), $C = 0.6\ \mathrm{W/mK}$ (thermal conductivity of water) and $I_{tot} = 1\ \mathrm{W}$. Note that the temperature increase at the assay, which is close to the surface, is less due to the high thermal conductivity of quartz

Parameter	Variable	Value (for $1\mu m$ polystyrene microsphere at 21°C)
Viscosity of medium	η	1.00 mPa s
Refractive index medium at 1070 nm	n_{med}	$1.32 + 10^{-6}i$
Refractive index polystyrene at 1070 nm	n_{poly}	$1.58 + 0i$
Refractive index melamine at 1070 nm	n_{mel}	$1.68 + 0i$
Refractive index titania at 1070 nm	n_{tit}	$2.50 + 0i$
Refractive index gold at 1070 nm	n_{gold}	$0.27 + 7.15i$
Density polystyrene	ρ_{poly}	1.05 g cm^{-3}
Density melamine	ρ_{mel}	1.57 g cm^{-3}
Density titania	ρ_{tit}	4.23 g cm^{-3}
Density gold	ρ_{gold}	19.3 g cm^{-3}
Viscous drag of microsphere	$\gamma = 6\pi R\eta$	9.42 pN s μm^{-1}
Average thermal microsphere velocity	$v_{th} = \sqrt{k_B T/m}$	2.71 mm s^{-1}
Reynolds number	$Re = Rv_{th}\rho/\eta$	$1.4 \cdot 10^{-3}$
Absolute permittivity of water	$\epsilon_0\epsilon_W$	$70.832 \cdot 10^{-13}\ \mathrm{Fm}^{-1}$
Effective surface potential	ψ_0	5 mV
Debye screening length	l	10 nm

Persistence length of DNA	L_p	50 nm
Stretch modulus of DNA	S	1500 pN

Supplementary Table 1: parameters used for calculations.

Supplementary figures

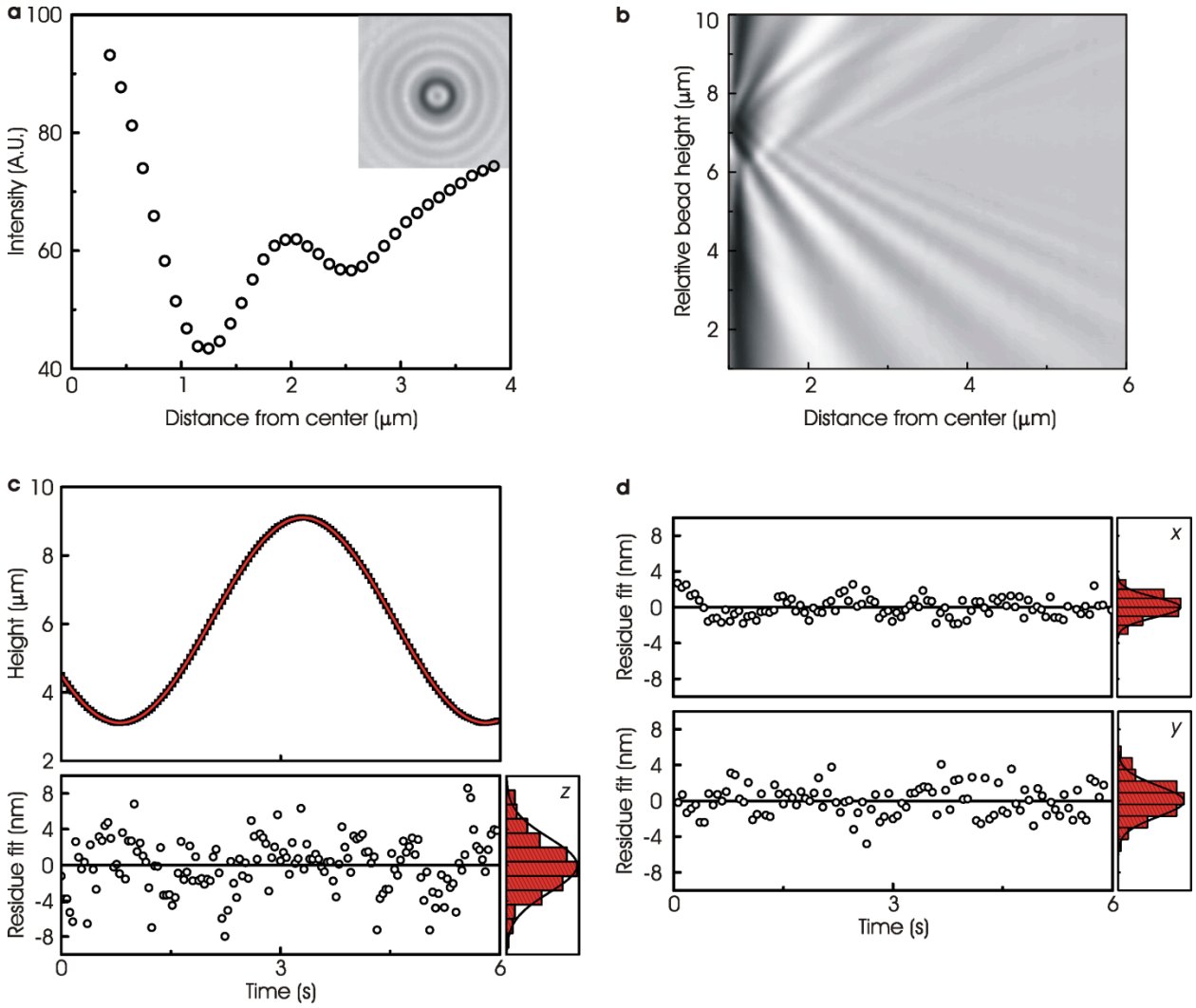

Supplementary Figure 1 | *Relative height determination of a microsphere using a look up table (LUT).* ***a.*** *Images of the microsphere (inset) are converted to a radial profile. Radial profiles of 6 images are averaged and binned over 100 nm. The radial profile is measured as a function of the microsphere height, using the piezo stage to control the height. (**b**) Stack of radial profiles as a function of the relative microsphere height. During a measurement the microspheres radial profile is compared to the radial profiles in the LUT to obtain the microspheres height.* ***c.*** *To determine the accuracy of our microsphere*

tracking in z (at 25 Hz) we measured the height of a stuck microsphere (2.1 um diameter) that is moved up and down in a sinusoidal manner using the piezo stage. The standard deviation of the residues from the sinusoidal fit of the height data is 4 nm, which is the accuracy we achieve in z. ***d.*** *The residues in the x- and y-dimension, determined in the same way as in* ***c*** *but moving the piezo stage in respectively x and y. In both these dimensions we achieve an accuracy of approximately 2nm (at 25 Hz).*

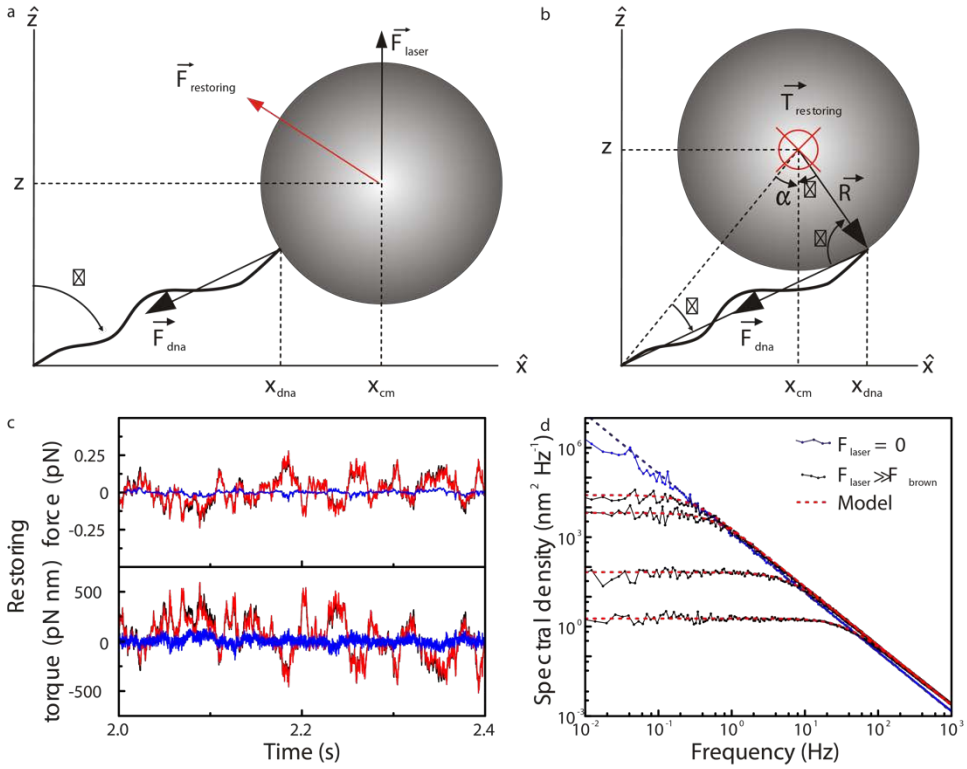

Supplementary Figure 2 | *Schematic overview of a DNA tether pushed out of its equilibrium position by the Brownian force.* ***a****. The displacement due to the Brownian motion leads to a small angle ϑ, giving rise to a restoring force. Note that there is also a difference between the observed center of the microsphere and the real attachment point of the DNA.* ***b****. The displacement and rotation of the microsphere (ϕ) lead to a different anchor point position of the DNA and to a restoring torque acting on the center of the microsphere. The angles α, β, ξ are introduced to assist the calculations.* ***c****. Comparison of the restoring torque and force for the linearized (red) and full model (black). The residuals (blue) are symmetrical and have a standard deviation of 0.01 pN and 26 pN·nm for the force and torque respectively.* ***d****. Power spectra of the simulated data sets and plots of the analytical model using the same parameters (ϕ 4.26 μm, 1.1 kbp DNA). The spectra from top to bottom are simulated and calculated using applied forces of 0 pN, 0.5*

pN, 1 pN, 10 pN, 60 pN for the spectra from top to bottom. The spectrum and plot in the absence of force is given in blue for reference.

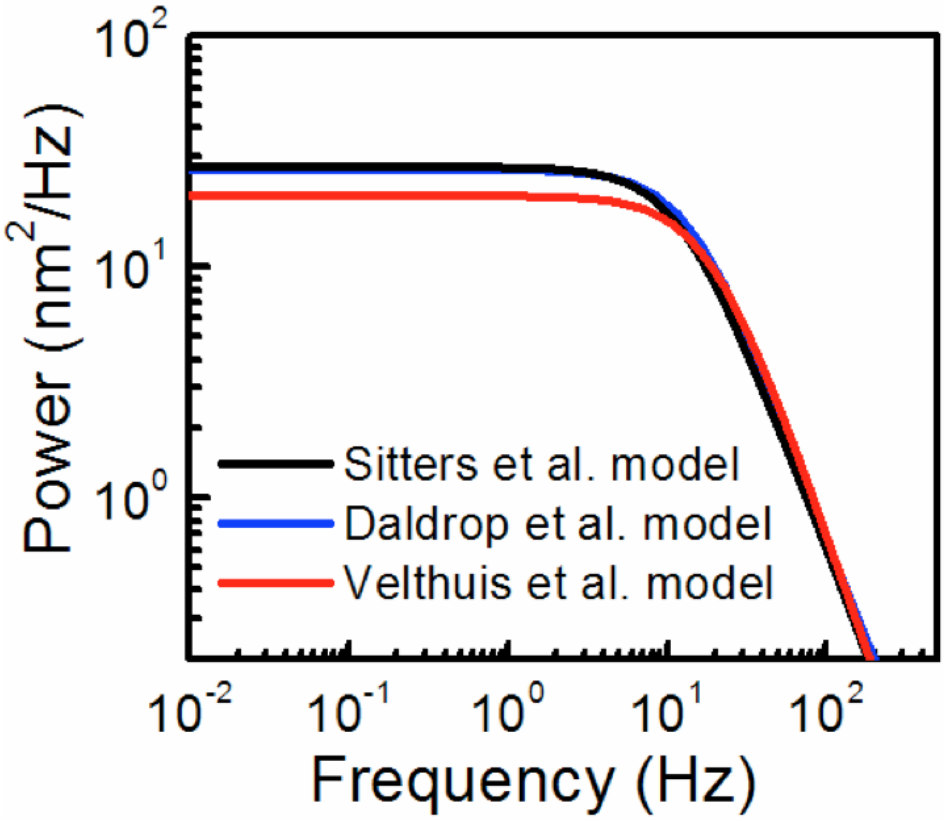

Supplementary Figure 3 | *Calculated power spectra of the Daldrop et al., Velthuis et al. and the model used in the paper for for a microsphere that is 3 µm in diameter, a DNA molecule with a contour length of 0.3 µm and an exerted force of 10 pN. The graph shows good agreement between the model used in the paper and the Daldrop model. The power spectrum calculated with the Velthuis model differs significantly below the cut of frequency.*

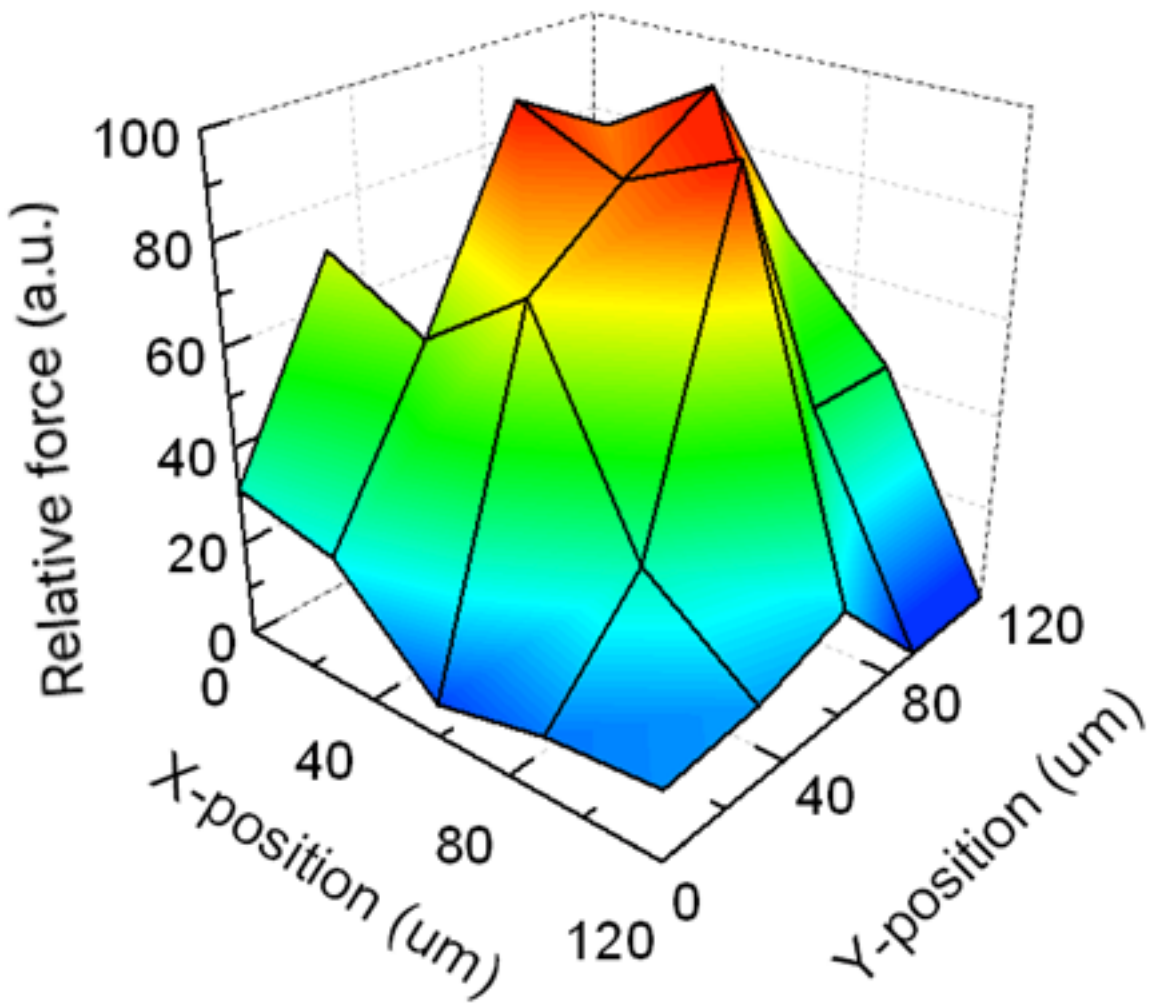

Supplementary Figure 4 | *The measured force profile within a field of view on the camera. This plot is acquired by measuring the force on the same bead at 25 different locations within the field of view using the same laser power. The profile has a FWHM of* 74 ± 9 nm (using a 2D Gaussian fit).

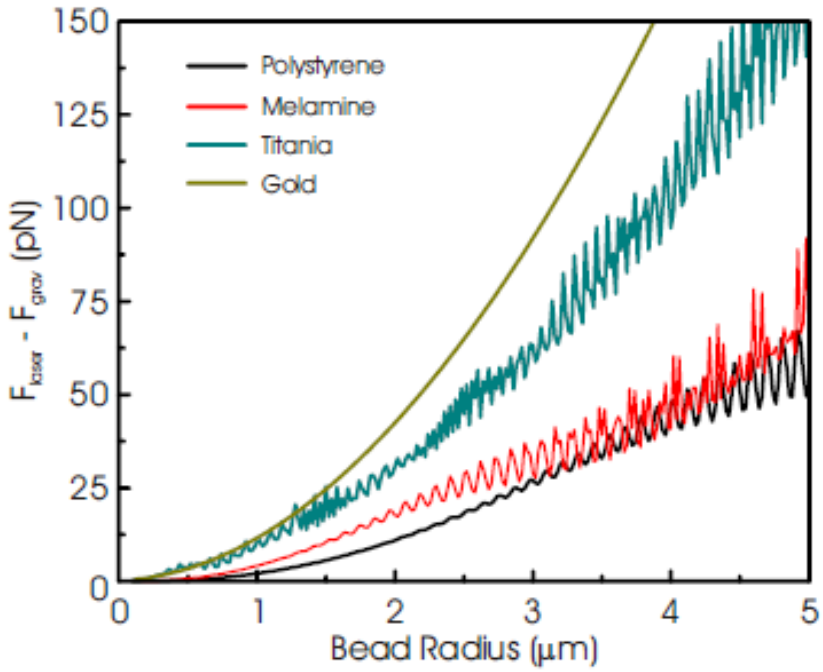

Supplementary Figure 5 | *The calculated optical pushing force for different materials using Mie theory (gravity force is substracted). In general materials with a higher refractive index experience a bigger force using the same intensity. Calculations were performed for particles in the center of a 1064nm, 100μm FWHM and 8W laser.*

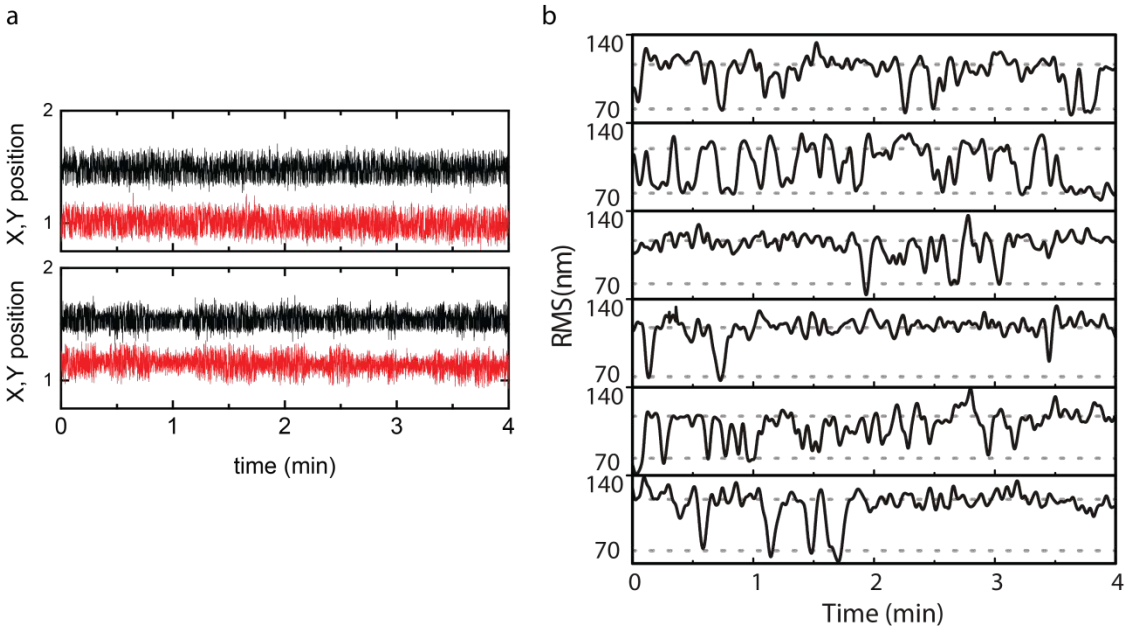

Supplementary Figure 6 | ***a***. *Raw data traces of the X (black) and Y (red) position of a tethered microsphere (ϕ 440 nm) in the absence (top) and presence (bottom) of the FokI restriction enzyme under a constant force of ~10 fN. If FokI is present, looping behavior is observed resulting in smaller bead motion in both dimensions.* ***b***. *Root mean square (RMS) traces (2s time window) of simultaneous measured microspheres under constant force of ~ 10 fN, show clear looping behavior (indicated by the dashed lines) in the presence of the FokI restriction enzyme. The length of the DNA in the unlooped state is 180 nm and I the looped state 115 nm.*

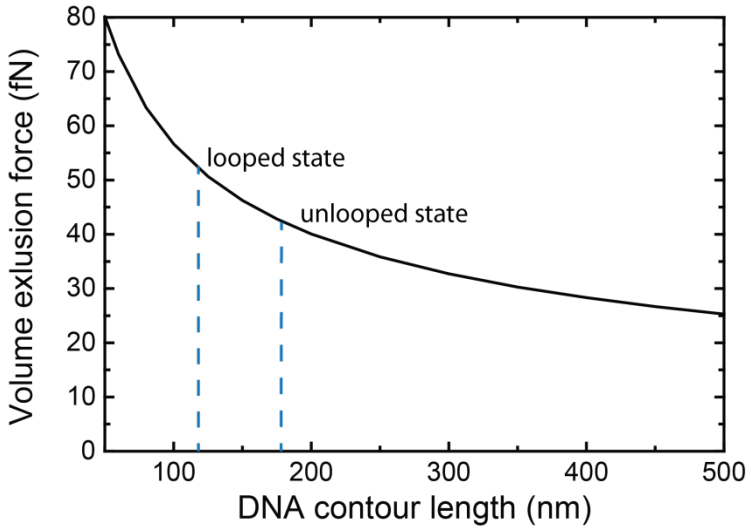

Supplementary Figure 7 | *The calculated volume exclusion force of a tethered microsphere (ϕ 440 nm) as a function of DNA contour length*[11]*. This plot shows that the volume exclusion force decreases less than 10 fN going from looped to unlooped state.*

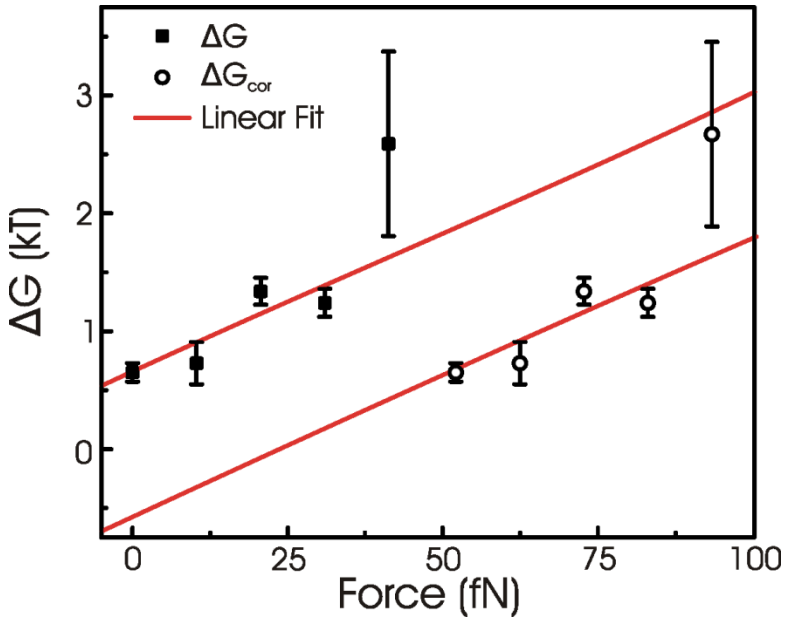

Supplementary Figure 8 | *Calculated free energy change ΔG at different forces for both the uncorrected and corrected forces (volume exclusion force taken into account). The linear fit is used to determine the standard free energy change* ΔG^0.

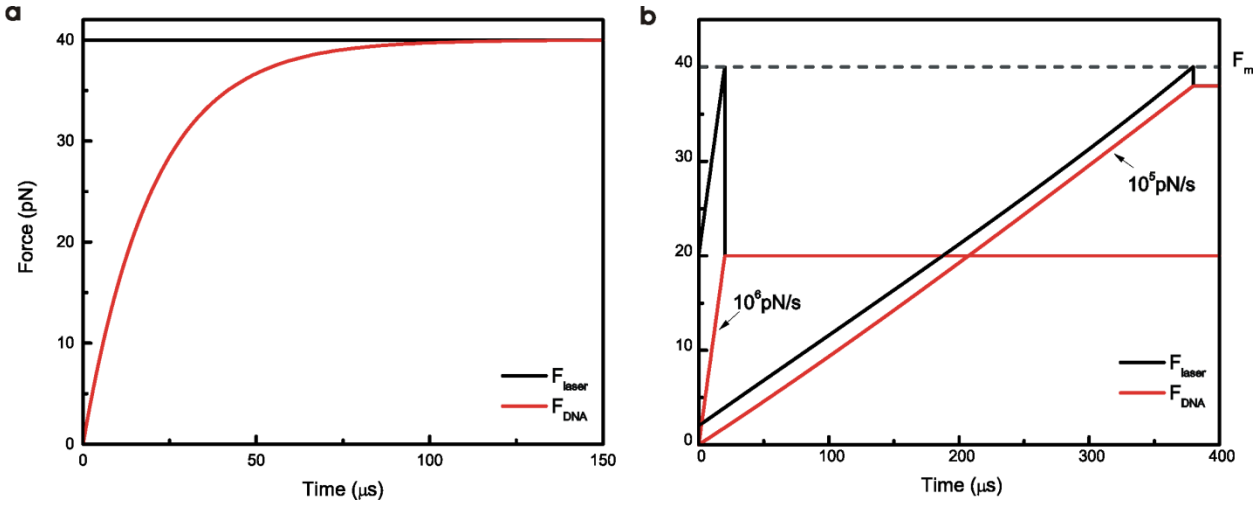

Supplementary Figure 9 | ***a.*** *Force response on the DNA ($L_c = 400nm$) if 40pN is applied instantaneously on the microsphere ($\phi\, 4.26\mu m$). The response time of the system is ~ 100μs.* ***b.*** *It is possible to achieve a linear force response on the DNA if an initial offset is applied to the force ramp of the laser. Note that a higher ramp results in a lower maximum force on the DNA.*

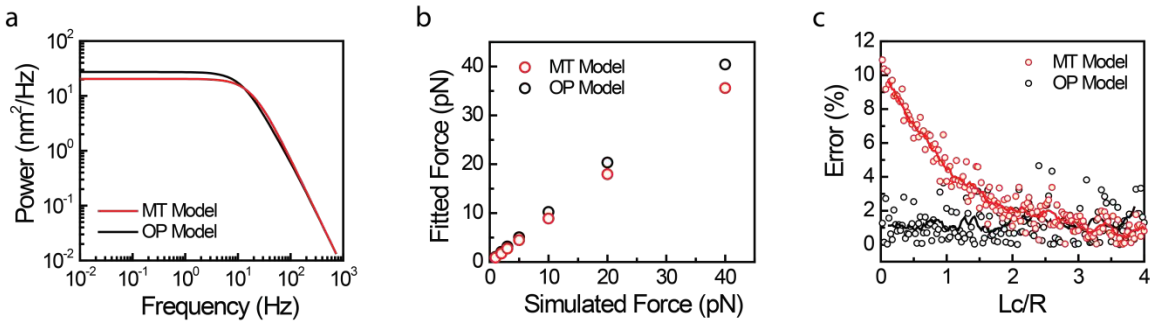

Supplementary Figure 10 | ***a.*** *Power spectra of the Magnetic Tweezer (MT) model (same as Velthuis et al mode in Supplementary Figure 3) and the Optical Pushing (OP) model (same as Sitters et al. model in Supplementary Figure 3) calculated for a microsphere that is 3 µm in diameter, a DNA with a contour length of 0.3 µm and a exerted force of 10 pN. The graph shows that the microspheres fluctuations are higher at lower frequencies if microsphere rotation is taken into account, leading to a higher plateau in the power spectrum for the OP case.* ***b.*** *Fitting power spectra of simulated data (acquired from trajectories of 600s) shows the MT model clearly underestimates the applied force, whereas the OP model predicts the forces accurately.* ***c.*** *The error of the fitted force (using 10pN) for simulated microsphere trajectories using the MT and the OP model. For microsphere-tether systems with* $L_c/R < 2$ *the OP model is clearly able to fit applied forces more accurately than the MT model.*

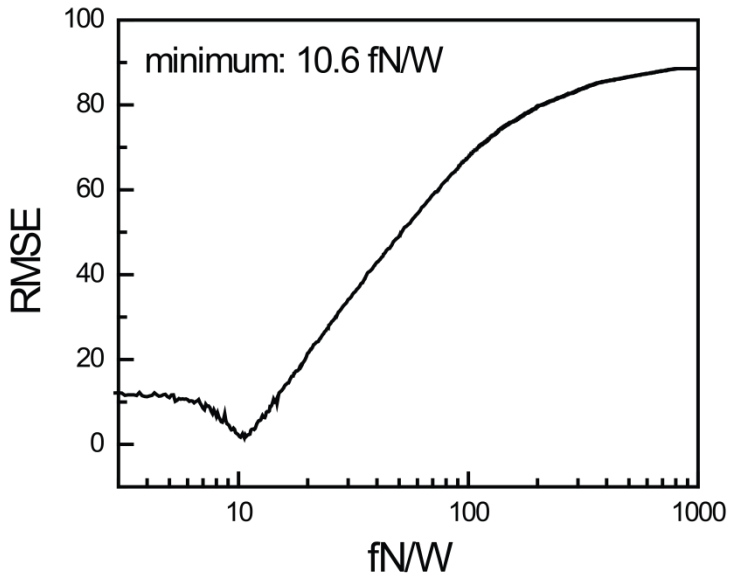

Supplementary Figure 11 | *The root mean squared error (RMSE) as a function of force calibration factor for the small beads (ϕ 440 nm). The minimum error corresponds to a calibration factor of 10.6 fN/W.*

(1) Te Velthuis, A. J. W.; Kerssemakers, J. W. J.; Lipfert, J.; Dekker, N. H. *Biophys. J.* **2010**, *99*, 1292–1302.

(2) Reif, F. *Fundamentals of statistical and thermal physics*; McGraw-Hill: Singapore, 1985.

(3) Howard, J. *Mechanics of motor proteins and the cytoskeleton*; 2001.

(4) Risken, H. *The Fokker-Plank Equation. Methods of Solution an Applications*; Springer Berlin Heidelberg: Berlin, 1989.

(5) Happel, J.; Brenner, H. *Low Reynolds Number Hydrodynamics*; Kluwer Academic Publishers: Dordrecht, The Netherlands, 1983.

(6) Marko, J. F.; Siggia, E. D. *Macromolecules* **1995**, *28*, 8759–8770.

(7) Schäffer, E.; Nørrelykke, S.; Howard, J. *Langmuir* **2007**, *287*, 3654–3665.

(8) *Absorption and Scattering of Light by Small Particles*; Bohren, C. F.; Huffman, D. R., Eds.; Wiley-VCH Verlag GmbH: Weinheim, Germany, 1998.

(9) Pawley, J. *Handbook of Biological Confocal Microscopy*; 3rd ed.; Springer Science + Business Media, 2006.

(10) Peterman, E. J. G.; Gittes, F.; Schmidt, C. F. *Biophys. J.* **2003**, *84*, 1308–1316.

(11) Segall, D.; Nelson, P.; Phillips, R. *Phys. Rev. Lett.* **2006**, *96*, 088306.